Available online at www.sciencedirect.com

ScienceDirect

Ceramics International 40 (2014) 1619–1625

CERAMICS INTERNATIONAL

www.elsevier.com/locate/ceramint

Characterization of rare earth oxide-rich glass applied to the glass-infiltration of a ceramic system

Cauê M.M. Bighetti[a], Sebastião Ribeiro[a], Simone Pereira T. Borges[b], Kurt Strecker[c], João Paulo B. Machado[d], Claudinei Santos[a,e,*]

[a]Universidade de São Paulo-Escola de Engenharia de Lorena, USP-EEL. Pólo Urbo-Industrial, Gleba AI-6, s/n, Lorena-SP, CEP 12600-000, Brazil
[b]Universidade Federal do Espírito Santo (UFES)-Alto Universitário, s/n Guararema, PO box 16, Alegre-ES, CEP 29500-000, Brazil
[c]Universidade Federal de São João Del Rei–Departamento de Engenharia Mecânica, UFSJ-DEMEC, Praça Frei Orlando. 170-Centro, São João Del Rei-MG, CEP 35353-353, Brazil
[d]Instituto Nacional de Pesquisas Espaciais, INPE/LAS, Av. dos Astronautas, 1758, São José dos Campos-SP, CEP 12227-010, Brazil
[e]Universidade do Estado do Rio de Janeiro, Faculdade de Tecnologia–UERJ-FAT, Rodovia Presidente Dutra, km 298, Resende-RJ, CEP 27511-971, Brazil

Received 15 February 2013; received in revised form 2 July 2013; accepted 11 July 2013
Available online 17 July 2013

Abstract

The viability of a silica glass containing rare earth oxides as infiltration agents in different ceramic substrates was investigated. $ZrO_2(Y_2O_3)$–Al_2O_3 and Al_2O_3–$ZrO_2(Y_2O_3)$ composite ceramics were sintered at 1530 °C/2 h and characterized by X-ray diffraction (XRD), dilatometry and atomic force microscopy (AFM). The wetting behavior of the substrates by rare earth glass was studied by the sessile drop method at temperatures of up to 1285 °C in an argon atmosphere. Both composites presented high relative density (close to 98%) with α-Al_2O_3 and tetragonal ZrO_2 as crystalline phases. The wetting angle of the two substrates decreased in response to increasing temperature, reaching a final contact angle of 12.7° on the $ZrO_2(Y_2O_3)$:Al_2O_3 substrate at 1285 °C and of 13.6° on the Al_2O_3:$ZrO_2(Y_2O_3)$ substrate at 1275 °C, indicating good wettability in both cases. Results of fracture toughness show KIC of 4.3 MPa m1/2 and 5.4 MPa m1/2 for $ZrO_2(Y_2O_3)$:Al_2O_3 and Al_2O_3:$ZrO_2(Y_2O_3)$ respectively. The theoretical residual stress in the two infiltrated composites were calculated based on the coefficient of thermal expansion of the substrates and glass. The $ZrO_2(Y_2O_3)$:$Al2O_3$ and Al_2O_3:ZrO2(Y_2O_3) composites showed calculated residual stresses of 36.5 MPa (tensile) and 252 MPa (compression), respectively, indicating that compressive residual stress contributes to increase the toughness of the glass-infiltrated composites.

Keywords: Wettability; Zirconia-alumina composites; Residual stress; Interface; Glass characterization

1. Introduction

A trend in dentistry is to substitute metal-based prostheses for ceramic materials, mainly due to esthetic reasons. Alumina-based ceramics, Al_2O_3, have high hardness and wear resistance, while yttrium stabilized zirconia-based ceramics, $ZrO_2(Y_2O_3)$, have high fracture toughness and strength and are esthetically more attractive [1]. The high fracture toughness of $ZrO_2(Y_2O_3)$ ceramics is due to the tetragonal-to-monoclinic phase transformation, accompanied by a 3 to 6 vol% expansion in grains. The stress-induced tetragonal-to-monoclinic ZrO_2 transformation ahead of a crack tip generates compressive stresses in the ceramic matrix, hindering crack propagation and thus resulting in high fracture toughness [2,3]. High toughness is a very important factor in dental materials due to the induced and alternating stresses to which they are subjected [1]. During mastication the loads are usually in the order of 200 N, but may reach up to 1200 N [4].

A method widely used to produce dental prosthesis is by CAD/CAM machining of pre-sintered ceramic blocks with subsequent infiltration of a glass into a porous substrate and final sintering to densification. In this case, it is important that the coefficient of thermal expansion (CTE) of the ceramic

*Corresponding author at: Universidade de São Paulo-Escola de Engenharia de Lorena, USP-EEL. Pólo Urbo-Industrial, Gleba AI-6, s/n, Lorena-SP, CEP 12600-000, Brazil. Tel. +55 24 33813839.
E-mail address: claudinei@pesqusiador.cnpq.br (C. Santos).

0272-8842/$ - see front matter © 2013 Elsevier Ltd and Techna Group S.r.l. All rights reserved.
http://dx.doi.org/10.1016/j.ceramint.2013.07.052

substrate and the glass present only slight differences in order to minimize thermal mismatch, which could lead to undesirable internal stress and cause cracking of the component during processing. Another important parameter is the contact angle between glass and substrate, which indicates the wettability of the glass in the ceramic and the possibility of full densification after infiltration.

The mechanical stability of dental prostheses is a critical factor, because the durability of the junction must be ensured. Zirconia-based ceramics may undergo tetragonal-to-monoclinic ZrO_2 phase transformation in aqueous or salty environments. An alternative to monoclinic ZrO_2-based ceramics, which does not involve tetragonal-to-monoclinic ZrO_2 phase transformation, are composite materials based on ZrO_2–Al_2O_3 mixtures [2,3] or ZrO_2-glass systems [5].

In the production of composites with phases exhibiting distinct characteristics, as in the case of ZrO_2–Al_2O_3 infiltrated by a glass, it is necessary to study the physical and chemical interactions between the constituents. For effective infiltration, the glass must wet the surface of the substrate. This behavior is commonly described by the wetting or contact angle, θ [6–9]. This contact angle is established as a result of the interfacial energies between the liquid and solid phases [10–13]. Wettability is described by Young′s Eq. (1).

$$-\Delta G = \gamma^{lv}(1 + \cos\,\theta) \tag{1}$$

where ΔG represents the Gibbs free energy and γ^{lv} represents the surface energies of liquid–vapor.

If θ equals zero, wetting is maximum and spreading of the liquid occurs; when θ equals 90°, partial wetting occurs, and when θ equals 180°, wetting does not occur. Therefore, a minimum contact angle is necessary for wetting to occur.

The most common method for determining wettability is the sessile drop method [6,14–18]. This method consists of heating a fusible material on a solid substrate and measuring the contact angle of the liquid drop on the substrate as a function of temperature and/or time. The variation in the height and diameter of the liquid drop is recorded continuously with a camera.

Based on the thermal expansion coefficients of the matrix and glass phase, residual stresses are generated between the substrate and the glass [19], as illustrated in Fig. 1

- $\alpha_{glass} > \alpha_{substrate}$: shrinkage of the matrix (substrate) is higher than that of the glass. The matrix/glass interface is thus stressed, leading to radial microcracks in the matrix around the glass.
- $\alpha_{glass} = \alpha_{substrate}$: no stresses appear at the interface, since the matrix and glass shrink equally.
- $\alpha_{glass} < \alpha_{substrate}$: shrinkage of the matrix (during cooling after sintering) is lower than that of the glass. To improve the fracture toughness, the intensity of the tensile stress must be limited to prevent partial or total interfacial debonding.

The average thermal residual stress generated during the cooling of sintered samples is calculated based on the assumption of a homogeneous distribution of secondary phase in the ceramic matrix obtained during infiltration, and is directly related to the difference in the coefficients of thermal expansion of the substrate and the glassy intergranular phase [20–22]. The average residual stress in both phases can be calculated as a function of the volume fraction of secondary phase, based on the approach proposed by Shi et al. [21], using Eqs. (2) and (3).

$$\sigma_g = E_g(\langle\alpha\rangle - \alpha_g)\Delta T \tag{2}$$

$$\sigma_m = E_m(\langle\alpha\rangle - \alpha_m)\Delta T \tag{3}$$

Here, σ_g and σ_m are residual stresses in the system (glass and substrate matrix, respectively). E_m and E_g indicate the Young modulus of the matrix and glass, respectively, and α, α_m and α_g indicate the average coefficient of thermal expansion (CTE) of the composite, matrix and glassy phase, respectively. The average coefficient of thermal expansion for each composition can be calculated using Eq. (4)

$$\langle\alpha\rangle = \frac{\alpha_g C_g E_g + \alpha_m C_m E_m}{C_g E_g + C_m E_m} \tag{4}$$

where C_g and C_m are, respectively, the fraction of glass and matrix. Based on the above calculation one finds that, on average, when $\alpha_m > \alpha_g$ and $\sigma_g < 0$, the grain boundary will be in compression and the matrix will be in tension [21,22]. Residual stress in multiphase composites develops due to the mismatch of the E-modulus and the coefficient of thermal expansion (CTE) in the constituent phases. Due to the lower CTE of the glass α_b than that of the matrix α_m, residual tensile stresses develop in the ZrO_2–Al_2O_3 matrix during cooling.

The purpose of this work was to investigate the compatibility of the rare earth oxide-rich glass with $ZrO_2(Y_2O_3)$–Al_2O_3 and Al_2O_3–$ZrO_2(Y_2O_3)$ ceramic composites based on an analysis of wettability and residual stress. The analysis

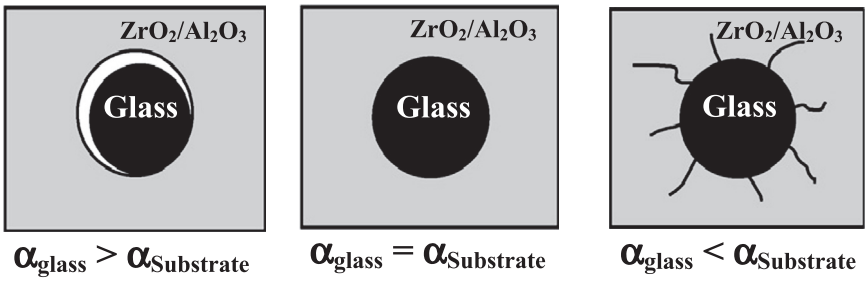

Fig. 1. Internal stresses and associated damage mechanisms involved during cooling by thermal expansion mismatch between spherical glasses embedded in a substrate.

confirmed the viability of this glass as an infiltration agent for ZrO_2–Al_2O_3 composites.

2. Experimental procedure

2.1. Processing

Pre-sintered ceramic substrates composed of 80:20 wt% ZrO_2(3 mol%Y_2O_3)–Al_2O_3 and 80:20 wt% Al_2O_3–ZrO_2(3 mol%Y_2O_3) (ProtMat Mat. Avançados, Brazil), herein referred to as Z8A2 and Z2A8, respectively, with green relative density near to 80% of theoretical density, were sintered at 1530 °C/2 h, applying a heating/cooling rate of 10 °C/min. The samples were cut into test specimens ($20 \times 20 \times 4$ mm^3), their surfaces ground and polished with diamond paste, washed with acetone in an ultrasonic bath for 10 min, and dried at 100 °C for 1 h.

Table 1 describes the chemical composition of the glass developed in this work.

The glass was produced by milling the oxides in isopropyl alcohol for 4 h, followed by drying and sieving of the mixture. The powder mixture was melted at 1550 °C for 30 min and heat-treated at 600 °C for 30 min, after which it was slowly cooled to room temperature. The resulting glass was cut into small $4 \times 4 \times 4$ mm^3 specimens and machined into 3 mm diameter cylinders. This sample geometry is recommended by the DIN 51730 standard [23], which considers that the melting point is reached when the liquid drop acquires a semi-spherical shape. The choice of this glass was based on its thermal compatibility with ceramic substrates.

Table 1
Chemical composition of the glass.

Components	Composition (in wt%)
Rare earth oxides (La_2O_3+Y_2O_3+CeO_2)	42.0
SiO_2+Al_2O_3	33.0
B_2O_3+CaO	19.0
TiO_2	4.0
ZrO_2	2.0

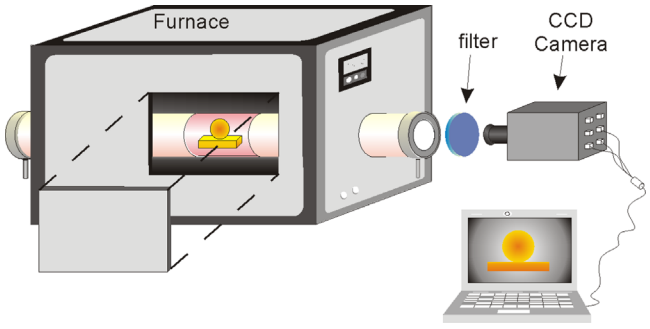

Fig. 2. Schematic diagram of the wettability test apparatus.

2.2. Characterization

The ceramic substrates were characterized based on their relative density, phase composition, surface roughness and microstructure. The relative densities were determined by the Archimedes method, relating the apparent density to the theoretical density. The apparent density, which was determined by helium pycnometry, was 5.48 g/cm^3 for the Z8A2 and 4.21 g/cm^3 for the Z2A8.

Crystalline phases (glass and substrates) were analyzed by X-ray diffraction, using CuKα radiation (λ=1.5418 Å) in the 2θ range of 10° to 90°, with a step width of 0.02° and 2 s of exposure time/point. The crystalline phases were determined by comparison with the JCPDS files [24].

Wettability, represented by the contact angle θ generated between the liquid glass and the substrate as a function of temperature, is strongly influenced by the surface roughness of the substrate. Therefore, the surface roughness was analyzed by atomic force microscopy (AFM), according the ISO 4287 standard [25]. The AFM analyses were conducted in the contact mode in air, using a V-shaped Si_3N_4 cantilever beam as sensor. Areas of 10,000 μm^2 were measured at a frequency of 0.5 Hz.

In addition, the glass/substrate interfaces were examined by scanning electron microscopy and the coefficient of thermal expansion (CTE) of the glass and substrates was determined by dilatometry, using a NETZSCH DIL 402 PC dilatometer.

2.3. Wettability test

The sessile drop method was used to study the wetting behavior of the glass on the substrate. The system consisted of a tubular electric furnace equipped with a CCD camera with a 4/50 mm lens, as shown schematically in Fig. 2. The camera was connected to a computer and the images were captured with a Matrox II YC +Mono device.

The glass samples were positioned on the polished substrate and heated at a rate of 10 °C/min in a flowing argon atmosphere. The tests lasted for about 120 min. The substrates

Table 2
Coefficient of thermal expansion (CTE) and Young Modulus of the substrates and glass.

Material	Coefficient of thermal expansion (CTE) (25 °C–800 °C)[a]	Young Modulus (GPa)
$ZrO_2(Y_2O_3)$ monolithic	10.6×10^{-6}/°C	200
Al_2O_3 monolithic	7.8×10^{-6}/°C	390
$ZrO_2(Y_2O_3)$–Al_2O_3	10.2×10^{-6}/°C	240
Al_2O_3–$ZrO_2(Y_2O_3)$	8.8×10^{-6}/°C	350
Rare earth glass	8.1×10^{-6}/°C	95

[a] T_g—Glassy transition temperature ~800 °C

were positioned on an alumina bar whose surface found himself perfectly horizontal in order to avoid errors in measurement or positioning of the glass sample. Images were captured at different temperatures and the contact angle was measured from these images, using Image Tool software. The values of instantaneous contact angles were measured only during heating, in order to simulate the conditions under which infiltration glasses will be subjected. In this work the angles of equilibrium for this system were not determined.

After the wetting tests, specimens were cut along the longitudinal plane and analyzed by scanning electron microscopy (SEM).

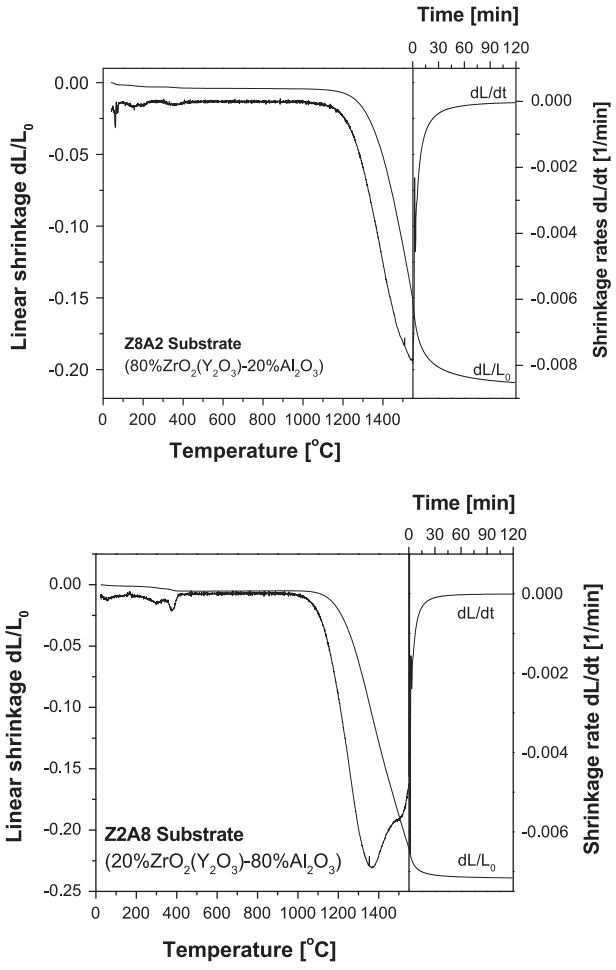

Fig. 3. Shrinkage and shrinkage rates of the substrate materials during sintering.

2.4. Infiltration testing

In pre-sintered ceramics, samples with $10 \times 10\ mm^2$ were cut. The thickness with 1.0 mm was standardized in order to approximate the conditions for thickness dimensions of the prosthesis. For mechanical properties, a sample of pre-sintered Al_2O_3 with porosity close to 20% and dimensions $10 \times 10 \times 1.0\ mm^3$ was prepared.

The specimens were subjected to ultrasonic cleaning using isopropyl alcohol as a vehicle for 60 s. The substrates were dried at 120 °C-2 h, and subjected to infiltration of glass powders (with particle sizes less than 32 mm). Slurry consisting of deionized water with glass powders was applied on the surface of larger section and the samples were subjected to the same heating furnace EDG—Aluminipress-Brazil, at 1175 °C with a heating rate of 10 °C/min under vacuum. After heating, the samples were immediately cooled with cooling rates of 5 °C/min.

2.5. Mechanical Properties

The cross-section of the infiltrated samples was polished. Hardness and fracture toughness (KIC), were determined using a Vickers Indentation method. In each sample, 20 indentations were measured, under a load of 1000 gf for 15 s. The fracture toughness has been calculated by measurement of the relation between cracks length (c) and indentation length (a), using the relation proposed by Niihara et al. [26], valid for Palmqvist crack types.

3. Results and discussion

3.1. Characterization of substrates and glass

Final relative densities of the Z8A2 and Z2A8 sintered substrates used in the wettability tests, were $98.9 \pm 1.6\%$ and $97.2 \pm 1.7\%$, respectively.

Table 2 describes the coefficients of thermal expansion (CTE) and the Young Modulus of the materials studied in this work. The dilatometry results indicate that the CTE of the substrates is higher than that of the glass. Furthermore, Fig. 3 depicts the dilatometry curves of the substrates. As can be seen, maximum shrinkage occurred between 1500 °C and 1550 °C, with the Z8A2 substrate showing a higher shrinkage rate than the Z2A8 composite. Therefore, the sintering temperature

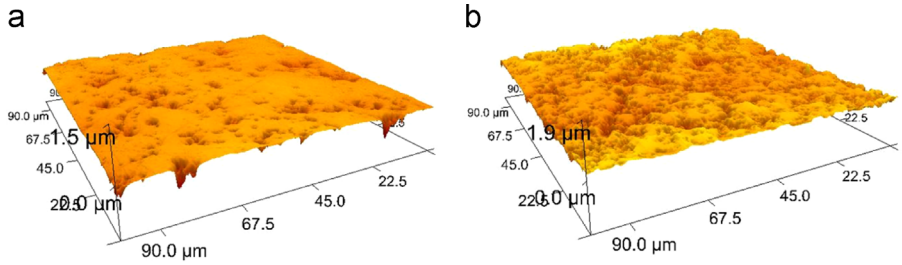

Fig. 4. AFM images of the surface roughness of the substrates (a) Z8A2 and (b) Z2A8.

for the Al_2O_3-rich-composite (Z2A8) should be increased to achieve a higher final density.

Fig. 4 depicts AFM images of the surface. The average roughness, *Ra*, of the Z8A2 substrate, determined from a total area of 30755 μm^2, was 105.5 ± 3.5 nm, while that of the Z2A8 substrate (total area of 30198 μm^2) was 55.2 ± 2.3 nm. Although the two substrate surfaces were polished in the same way, their average surface roughness differed considerably, as clearly shown in the AFM images in Fig. 4. However, the surface roughness was considered negligible, even in the case of the Z2A8 substrate, since it did not significantly influence the wetting behavior of the liquid glass.

Fig. 5 shows X-ray diffraction patterns of glass and two substrate materials. Tetragonal ZrO_2 and α-Al_2O_3 (corundum) were identified as crystalline phases in both substrates, Fig. 5a. The Al_2O_3-peaks were more intense in the Z2A8 substrate than in the Z8A2 substrate, which was expected due to the higher Al_2O_3 content of the former. The XRD pattern of the rare earth glass, Fig. 5b, is a typical amorphous spectrum, indicating no crystalline phase in this material.

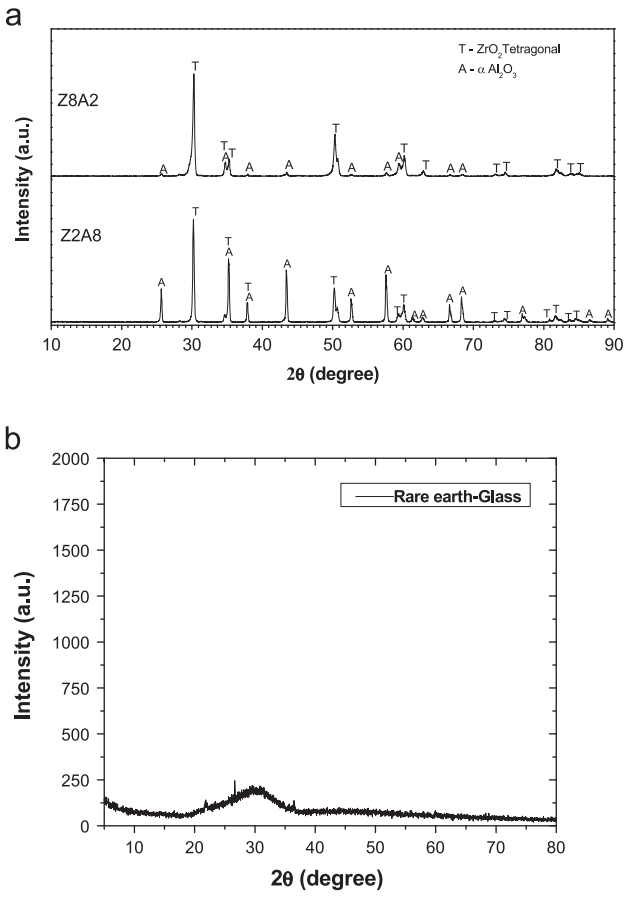

Fig. 5. X-ray diffraction patterns of the glass, Z8A2 and Z2A8 substrate.

3.2. Wettability Tests

Fig. 6 presents representative sequence photographs obtained during the wettability experiments on the Z2A8 substrate. As can be seen, the contact angle decreased with increasing temperature when the melted glass wet the substrate. According to the DIN 51730 standard, the melting point is reached when the sample presents the shape of a half sphere, which, in the case of the glass under study, occurred at approximately 1265 °C.

Fig. 7 shows the contact angles on the two substrates as a function of temperature. Note that the contact angles on both substrates decreased as the temperature increased. The figure also indicates that the two substrates showed a similar wetting rate, but which occurred at a slightly lower temperature on the Z8A2 substrate.

Based on these results, and after a mathematical adjustment of the sigmoidal curves, mathematical relations are proposed to describe the wettability (contact angle, θ) of the rare earth glass on the ZrO_2–Al_2O_3 (Z8A2 and Z2A8) substrates as a function of temperature (T), in Eqs. (5) and (6):

$$\theta_{Z8A2} = 9.2 + \frac{78}{1 + e^{-0.17(1259.5-T)}} \quad (5)$$

$$\theta_{Z2A8} = 9.7 + \frac{74.4}{1 + e^{0.20(1268.6-T)}} \quad (6)$$

The change in contact angle with increasing temperature follows a sigmoidal behavior and is described by Eq. (5) for the Z8A2 substrate, and by Eq. (6) for the Z2A8 substrate. A final contact angle of 12.7° on the Z8A2 substrate was reached at 1285 °C and of 13.6° on the Z2A8 substrate at 1275 °C. These contact angles are considered to be quite low. Hence, the glass presented good wettability on the substrates in question.

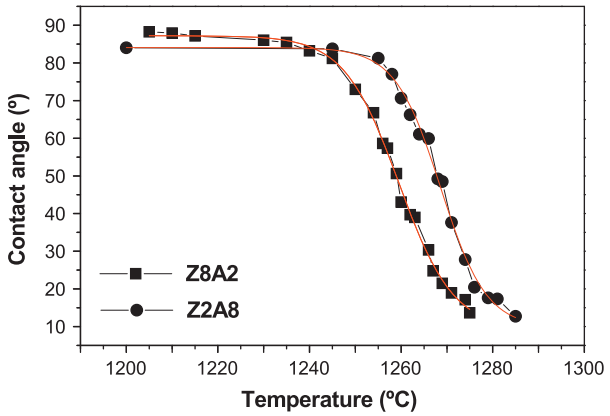

Fig. 7. Glass wetting behavior of Z8A2 and Z2A8 substrates as a function of temperature.

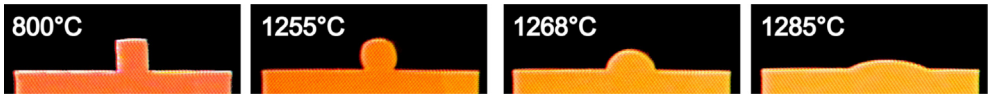

Fig. 6. Representative images obtained during the wettability test on the Z2A8 substrate.

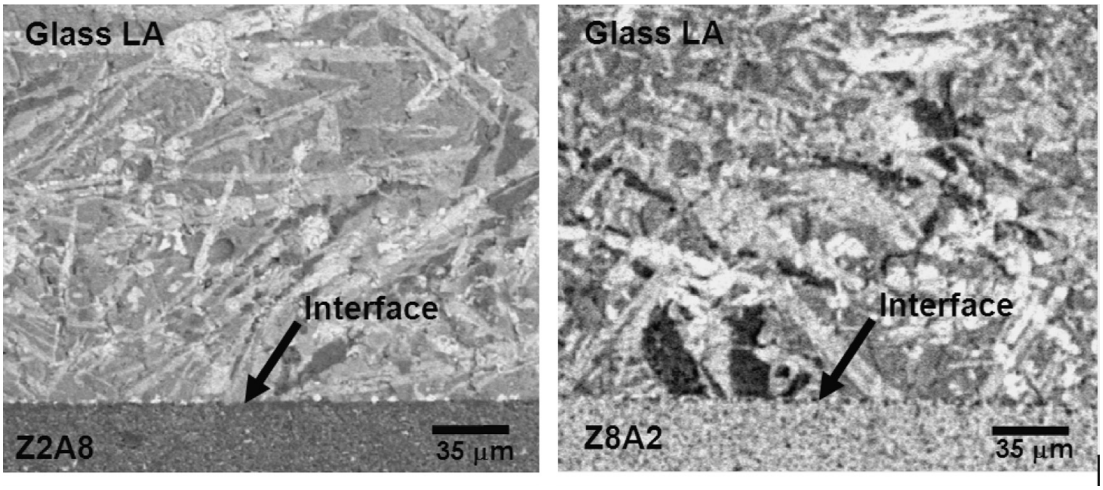

Fig. 8. SEM micrographs of cross-sections recorded after wettability experiments.

Table 3
Vickers hardness and fracture toughness of the infiltrated samples.

Composite	Vickers hardness (HV1000 gF)	Fracture toughness (MPa m1/2)	Theoretical thermal residual stress (MPa)
Al_2O_3–Glass	1138 ± 45	2.6 ± 0.4	5.4 MPa (tensile)
Z2A8-Glass	1065 ± 40	5.4 ± 0.3	252 MPa (compression)
Z8A2-Glass	985 ± 41	4.3 ± 0.4	36.5 MPa (tensile)

Fig. 8 shows SEM micrographs of the cross-sections recorded after the wetting tests. As can be seen, the glass/substrate interface remained flat, indicating that the substrate did not dissolve into glass. Furthermore, the absence of a reaction layer indicates that no chemical reaction occurred between the glass and substrate. Therefore, the wettability in this case is a purely physical phenomenon, following the Young′s Eq. (1). The glass did not show micro-cracking or phase separation from the substrates, indicating good adherence. This was attributed to the fact that the difference between the thermal expansion coefficients of the substrate, $\alpha_{Z8A2} = 10.2 \times 10^{-6}/°C$, or $\alpha_{Z2A8} = 8.8 \times 10^{-6}/°C$ and the glass, $\alpha_{glass} = 8.1 \times 10^{-6}/°C$, was insufficient to cause damage at the interface.

3.3. Residual stresses and mechanical Properties

The theoretical residual stress in the ceramic matrix was calculated according to the model proposed by Taya et al. [20]. In the calculations, E-moduli of 95 GPa, 240 MPa and 350 MPa were used for the rare earth glasses ZrO_2–Al_2O_3 and Al_2O_3–ZrO_2, respectively.

Systems that combine composite substrate with intergranular glassy phase have a higher level of complexity for discussion. Based on this analysis, in this work the discussion of residual stress is based initially on the study of residual stress between the components of the composite matrix, and then the presence of the glass phase as the secondary phase substrate.

In the $ZrO_2(Y_2O_3)$–Al2O3 and Al_2O_3–$ZrO_2(Y_2O_3)$ composite were used data presented in Table 2, and applied in Eqs. (2)–(4), to obtain the residual stress of the composites in the ranges of temperatures studied in infiltration tests (ΔT=1175 °C).

Calculations indicate that the composites Z2A8 have a compressive residual thermal stress of about 458 MPa, while the composite Z8A2 has tensile residual thermal stress of 423 MPa. From a mechanical standpoint, the toughening effect should be more relevant in the composite Z2A8 that the Z8A2 composite due to the compressive nature of stresses generated.

To calculate residual stress between the composite substrate and the glassy phase, the temperature range (ΔT) considered was the glass transition temperature indicated in dilatometry analysis to room temperature, in the order of 800 °C, below which the system is considered as rigid and therefore residual stresses are created materials.

The results of the calculated residual thermal stress indicates that the Z2A8 composite containing 20 vol% of glass has compressive residual stress of approximately 252 MPa, whereas the composite Z8A2 containing 20 vol% glass has residual thermal stress (tensile) calculated of around 36.5 MPa.

The results of the hardness and fracture toughness of the composites which presented full density after infiltration tests, are presented in Table 3.

Analyzing the Vickers hardness results, it was noted that the highest values are proportional to the greater amount of Al_2O_3 in the ceramic matrix, since the hardness of the Al_2O_3 is about 1800 HV, while ZrO_2 (Y_2O_3) has hardness near to 1300 HV.

It is observed that the composite Z2A8-Glass provides the best results of fracture toughness, near to 5.5 MPa m1/2.

.Comparing these results with values obtained for the composites Z8A2-Glass K_{IC} MPa m1/2) or $Al_2O_3K_{IC}$ MPa m1/2), it is

observed that materials with compressive residual thermal stresses have the most significant fracture toughness gains.

From the point of view of toughening mechanisms acting in these materials, it is noteworthy that the presence of tetragonal zirconia shown in Fig. 5a shows that there is greater possibility for phase-transformation toughening in composites Z8A2 because there is a larger population of grains of tetragonal-ZrO_2 in the other composites.

However, existing intergranular glassy phase, the cracks propagation preferably occurs by the grain boundaries.

Thus, the presence of compressive residual thermal stresses makes of this mechanism is more important that the phase-transformation toughening mechanism, common in tetragonal zirconia ceramic.

4. Conclusions

The rare earth glass presented high wettability in substrates of the $ZrO_2(Y_2O_3)$–Al_2O_3 composite system. Contact angles of 12.7° and 13.6° were identified for $ZrO_2(Y_2O_3)$–Al_2O_3 and Al_2O_3–$ZrO_2(Y_2O_3)$, respectively, indicating good glass infiltration in the zirconia–alumina composites. The coefficient of thermal expansion (CTE) of the glass and substrates was compatible, minimizing the formation of cracks which can cause defects in ceramics during processing. The slight difference in the CTE of the glass and matrix produced a residual compressive stress in the ceramic systems, preventing crack propagation and improving their strength. The wettability and residual compressive stress between glass and ceramic matrix indicate the feasibility of using this glass composition as a infiltration agent in $ZrO_2(Y_2O_3)$–Al_2O_3 and Al_2O_3–$ZrO_2(Y_2O_3)$ substrates.

Acknowledgments

The authors would like to thank the Brazilian research funding agency FAPESP (Fundação de Amparo à Pesquisa do Estado de São Paulo) for its financial support of this work (Grants 01/10664-6, 04/04386-1 and 08/00310-1).

References

[1] T.S. Hin, Engineering Materials for Biomedical Applications, World Scientific, Singapore, 2004.
[2] S.R. Choi, N.P. Bansal, Mechanical behavior of zirconia/alumina composites, Ceramics International 31 (2005) 39–46.
[3] E. Jimínez-Píqué, A. Domínguez-Rodríguez, J. Martinez-Fernandez, E. Lara-Curzio, M. Singh, Microstructure and mechanical properties of superplastically joined yttria–partially-stabilized zirconia (Y-TPZ) Ceramics, Journal of the European Ceramic Society 20 (2000) 39–46.
[4] A.R. Curtis, A.J. Wright, G.J.P. Fleming, The influence of simulated masticatory loading regimes on the bi-axial flexure strength and reliability of a Y-TZP dental ceramic, Journal of Dentistry 34 (5) (2006) 317–325.
[5] C. Santos, R.C. Souza, N. Almeida, F.A. Almeida, R.R.F. Silva, M.H.F. V. Fernandes, Toughened ZrO2 ceramics sintered with a La2O3-rich glass as additive, Journal of Materials Processing Technology 200 (2008) 126–132.
[6] A.M. Hadian, A.L. Drew, Thermodynamic modeling of wetting at silicon nitride/Ni–Cr–Si alloy interfaces, Materials Science and Engineering: A 189 (1994) 209–217.
[7] N. Siddqi, B. Bhoi, R.K. Paranguru, V. Sahajwalla, O. Ostrovski, Effect of the different parameters on wettality of graphite by CaO–SiO_2–Al2O_3–FeO–MgO slag, Transactions of the Indian Institute of Metals 53 (4-5) (2000) 479–486.
[8] M. Gindl, A comparison of different methods to calculate the surface free energy of Wood using contact angle measurements, Colloids and Surfaces A 181 (2001) 279–287.
[9] W.D. Kingery, Sintering in the presence of a liquid phase (1957) 235.
[10] S. Ribeiro, S.P. Taguchi, F.V. Motta, R.M. Balestra, The wettability of SiC ceramics by molten E_2O_3(ss)/AlN (E_2O_3(ss)) solid solution of rare earth oxides, Ceramics International 33 (2007) 527–530.
[11] R.M. Balestra, S. Ribeiro, S.P. Taguchi, F.V. Motta, C. Bormio-Nunes, Wetting behaviour of Y_2O_3/AlN additive on SiC ceramics, Journal of the European Ceramic Society 26 (2006) 3881–3886.
[12] F.V. Motta, R.M. Balestra, S. Ribeiro, S.P. Taguchi, Wetting behavior of SiC ceramics: Part I—E_2O_3/Al_2O_3 additive system, Materials Letter 58 (2004) 2805–2809.
[13] S.P. Taguchi, F.V. Motta, R.M. Balestra, S. Ribeiro, Wetting behavior of SiC ceramics: Part II—Y_2O_3/Al_2O_3 and Sm_2O_3/Al_2O_3, Materials Letter 58 (2004) 2810–2814.
[14] P. Xiao, B. Derby, The wetting of silicon nitride by chromium-containing alloys, Journal of Materials Science 30 (1995) 5915–5922.
[15] D.S. Han, H. Jones, H.V. Atkinson, The wettability of silicon-carbide by liquid aluminum—the effect of free alloy additions to the aluminum, Journal of Material Science 28 (10) (1993) 2654–2658.
[16] J.G. Li, H. Hausner, Wetting and adhesoin in liquid silicon ceramic system, Materials Letters 14 (5-6) (1992) 329–332.
[17] C.J. Lopez, H. Jones, H.V. Atkison, Wettability of silica substrates by silver-copper based brazing alloys in vacuo, Journal of the American Ceramic Society 83 (12) (2000) 2913–2918.
[18] M.I. Pech-Canul, R.N. Katz, M.M. Makhtouf, Optimum parameters for wetting silicon carbide by aluminum alloys, Materials Science and Engineering: A 31 (2) (2000) 565–573.
[19] M.G. Kakroudi, M. Huger, C. Gault, T. Chotard, Anisotropic behavior of andalusite particles used as aggregates on refractory castables, Journal of the European Ceramic Society 29 (4) (2009) 571–579.
[20] M. Taya, S. Hayashi, A.S. Kobayashi, H.S. Yoon, Toughening of a particulate-reinforced ceramic-matrix composite by thermal residual stress, Journal of the American Ceramic Society 73 (5) (1990) 1382–1391.
[21] J.L. Shi, Z.L. Lu, J.K. Guo, Model analysis of boundary residual stress and its effect on toughness in thin boundary layered yttria-stabilized tetragonal zirconia polycrystalline ceramics, Journal of Material Research 15 (3) (2000) 727–732.
[22] J.L. Shi, L. Li, J.K. Guo, Boundary stress and its effect on toughness in thin boundary layered and particulate composites: model analysis and experimental test on T-TZP based ceramic composites, Journal of the European Ceramic Society 18 (1998) 2035–2043.
[23] DIN 51730 standard: Deutsches Institut Fur Normung E.V. (German National Standard)/01-Sep-2007.
[24] Powder Diffraction File Inorganics Phases: alphabetical index, inorganics phases, JCPDS/international centre for diffraction data, Swarthmore, Pennsylvania, 1979.
[25] ISO 4287 International Organization for Standardization - Geometrical Product Specifications (GPS)—Surface texture: Profile method—Terms, definitions and surface texture parameters, 1997.
[26] K.A. Niihara, Fracture mechanics analysis of indentation-induced Palmqvist crack in ceramics, Journal of Materials Science Letter 2 (1983) 221–223.